


## ARTICLE

# $\mu$ -Conotoxin KIIIA peptidomimetics that block human voltage-gated sodium channels

Astrid Knuhtsen<sup>1</sup> | Rachel Whiting<sup>2</sup> | Fergus S. McWhinnie<sup>1</sup> |  
Charlotte Whitmore<sup>2</sup> | Brian O. Smith<sup>3</sup> | A. Christopher Green<sup>2</sup> |  
Christopher M. Timperley<sup>2</sup> | Kenneth I. Kinnear<sup>2</sup> | Andrew G. Jamieson<sup>1</sup> 

<sup>1</sup>School of Chemistry, Joseph Black Building, University of Glasgow, Glasgow, UK

<sup>2</sup>Chemical, Biological and Radiological Division, Defence Science and Technology Laboratory, Porton Down, Salisbury, Wiltshire, UK

<sup>3</sup>Institute of Molecular, Cell & Systems Biology, College of Medical, Veterinary & Life Sciences, Joseph Black Building, University of Glasgow, Glasgow, UK

## Correspondence

Andrew G. Jamieson, School of Chemistry, Joseph Black Building, University of Glasgow, Glasgow, G12 8QQ UK.  
Email: andrew.jamieson.2@glasgow.ac.uk

## Funding information

University of Glasgow, DSTL, Grant/Award Numbers: DSTL/AGR/R/CBRN/01, DSTLX-1000141308; EPSRC, Grant/Award Number: EP/R511705/1

## Abstract

Peptidomimetics designed to target voltage-gated sodium channels have attracted significant attention as potential analgesics. However, voltage-gated sodium channel (VGSC)-blocking activity of these compounds has mainly been assessed using rat and/or mice homologs. In this study, we developed a novel series of conformationally constrained peptidomimetic analogues of the  $\mu$ -conotoxin KIIIA and assessed their activity against human VGSCs. Two of the mimetics block the currents of hNa<sub>v</sub>1.4 and hNa<sub>v</sub>1.6 channels. NMR derived structures of the mimetics provided excellent insight into the structural requirements for bioactivity. A lactam-constrained analogue, previously reported to be active in mice, did not block the corresponding human VGSC. This work highlights important differences in VGSCs between species and validates the potential of peptidomimetics as human analgesics.

## 1 | INTRODUCTION

Conotoxin peptides are isolated from the venom of fish hunting marine snails, which use them as an efficient means of prey incapacitation and as an effective defense mechanism. Conotoxin venom has been reported to have caused several human fatalities<sup>[1–3]</sup> and can pose a risk to human health.<sup>[4]</sup> However, conotoxins and their synthetic mimetics have attracted a substantial amount of interest due to their properties as selective chemical probes that target ion channels and receptors.<sup>[5–8]</sup> They are potential therapeutic leads for several clinical applications including the treatment of neuropathic pain,

hypertension and type 2 diabetes.<sup>[9]</sup> Ziconotide, a synthetic analogue of the conotoxin peptide  $\omega$ -MVIIA is licensed for clinical use in the treatment of severe and chronic pain.<sup>[10]</sup> Due to unfavorable physicochemical properties of the native peptides the development of conotoxin peptidomimetics has been an active field of study by academics and the pharmaceutical industry.<sup>[11]</sup> Development of new peptidomimetic chemistries that can be used to overcome the physicochemical limitations of native peptides and provide peptide leads for drug discovery are a high priority. This is generally achieved by chemically modifying the peptide structure, removing the vulnerable functionalities and introducing mimetic features to retain the overall three-dimensional bioactive conformation of the peptide.

$\mu$ -Conotoxin KIIIA ( $\mu$ -KIIIA) is isolated from the venom of the marine cone snail *Conus kinoshitai*.<sup>[12]</sup> The peptide primary sequence contains 16 amino acid residues that are constrained by three disulfide bonds to adopt an  $\alpha$ -helical secondary structure. As with other

Content includes material subject to © Crown copyright (2020), Dstl. This material is licensed under the terms of the Open Government Licence except where otherwise stated. To view this licence, visit <http://www.nationalarchives.gov.uk/doc/open-government-licence/version/3> or write to the Information Policy Team, The National Archives, Kew, London TW9 4DU, or email: [psi@nationalarchives.gsi.gov.uk](mailto:psi@nationalarchives.gsi.gov.uk).

This is an open access article under the terms of the Creative Commons Attribution License, which permits use, distribution and reproduction in any medium, provided the original work is properly cited.

© 2020 The Authors. *Peptide Science* published by Wiley Periodicals LLC

$\mu$ -conotoxins,  $\mu$ -KIIIA modulates the activity of voltage-gated sodium channels (VGSCs) by occluding the pore in the middle of the channel. VGSCs are heterotrimeric protein complexes composed of one  $\alpha$ -subunit and two  $\beta$ -subunits that form a single pore. The ion-conducting core subunits ( $\alpha$ -subunits) are solely required for voltage-dependent ion permeation, and the  $\beta$ -subunits are responsible for regulating membrane trafficking and channel properties.<sup>[13]</sup> Nine different subtypes of the  $\alpha$ -subunit of VGSCs have been identified in humans: Na<sub>v</sub>1.1–Na<sub>v</sub>1.9. Subtypes Na<sub>v</sub>1.1, Na<sub>v</sub>1.2, Na<sub>v</sub>1.3, and Na<sub>v</sub>1.6 are primarily located in the central nervous system (CNS). Na<sub>v</sub>1.4 functions in skeletal muscle and Na<sub>v</sub>1.5 in the heart. Na<sub>v</sub>1.7, Na<sub>v</sub>1.8, and Na<sub>v</sub>1.9 are mainly found in the peripheral nervous system.

The first structure of a human VGSC (Na<sub>v</sub>1.4- $\beta$ 1 complex) was solved to 3.2 Å resolution using cryo-electron microscopy in 2018.<sup>[14]</sup> This was followed in 2019 by the cryo-EM structure of  $\mu$ -KIIIA bound to human VGSC Na<sub>v</sub>1.2.<sup>[15]</sup> The cryo-EM structure of human Na<sub>v</sub>1.7 in complex with auxiliary subunits and animal toxins has also recently been reported.<sup>[16]</sup> These structures provide detailed information on the molecular mechanisms of VGSC blocking by peptide ligands and may potentially facilitate VGSC structure-based drug discovery.

Subtype Na<sub>v</sub>1.7 has been identified as a therapeutic target for the treatment of pain through genetic association with gain-of-function mutations in the SCN9A gene as the basis of inherited pain syndromes, including erythromelalgia and paroxysmal extreme pain disorder.<sup>[17]</sup>  $\mu$ -KIIIA has rank order selectivity of Na<sub>v</sub>1.4 ( $48 \pm 6$  nM)  $\geq$  Na<sub>v</sub>1.2 ( $61 \pm 5$  nM)  $>$  Na<sub>v</sub>1.6 ( $183 \pm 31$  nM)  $>$  Na<sub>v</sub>1.3 ( $3.6 \pm 0.3$   $\mu$ M), and has no effect on Na<sub>v</sub>1.5 and Na<sub>v</sub>1.8 (at 10  $\mu$ M).<sup>[18]</sup>

Numerous peptidomimetic strategies have been applied to  $\mu$ -conotoxins including peptide sequence miniaturization,<sup>[19]</sup> N- and C-terminal extension,<sup>[20]</sup> chimeras,<sup>[21]</sup> and small molecule mimetics.<sup>[22]</sup> Previous research by Norton and co-workers examined the effect of  $\mu$ -KIIIA peptidomimetics, incorporating a lactam conformational constraint, on the VGSC subtypes Na<sub>v</sub>1.1–1.9.<sup>[23]</sup> A [D9K13]-lactam analogue was identified with an IC<sub>50</sub> of 54  $\mu$ M against rat Na<sub>v</sub>1.4 and 40  $\mu$ M against mouse Na<sub>v</sub>1.6.<sup>[23]</sup>

This synthetic peptidomimetic strategy provides ready access to analogues to determine structure-activity-relationships and information on key functionalities required for the selective interaction with this important class of therapeutic target.<sup>[23]</sup> However, one limitation of previous studies is the use of rat and/or mouse sodium channels. Although rodent and human voltage-gated sodium channels have a high degree of amino acid sequence homology (ex. 92% sequence homology between human and rat Na<sub>v</sub>1.4), their sensitivity to ligands often differs between species.<sup>[24]</sup> The origin of these differences in many cases has yet to be elucidated, yet is likely to be revealed as more ion-channel structures are solved. The use of human VGSCs, expressed in human cells would give the most relevant data to underpin and expedite a medicinal chemistry programme.

The aim of the present work was to investigate whether synthetic conformational constraints could replace the complex disulfide bond bridging network in the  $\mu$ -KIIIA conotoxin peptide, and produce more stable analogues that would retain bioactivity against human VGSCs.

## 2 | MATERIALS AND METHODS

### 2.1 | General information

Standard Fmoc-protected amino acids were purchased from CEM Corporation or Pepceuticals and 2-(6-chloro-1H-benzotriazole-1-yl)-1,1,3,3-tetramethylammonium hexafluorophosphate (HCTU), peptide grade dimethyl formaldehyde (DMF) and ethyl (hydroxyimino) cyanoacetate (Oxyma Pure) were purchased from Pepceuticals. (R)-N-Fmoc- $\alpha$ -(7-octenyl)alanine was purchased from Nagase Europe (GmbH) and (S)-N-Fmoc- $\alpha$ -(4-pentenyl)alanine was purchased from Sigma Aldrich. Fmoc-Asp(O-2-PhiPr)-OH and Fmoc-Lys(Mmt)-OH were purchased from Merck. 2,4,6-Triisopropylbenzenesulfonyl hydrazide (TPSH) was purchased from TCI Chemicals. All other reagents were purchased from Sigma Aldrich.

Flash column chromatography was performed on a Biotage Isolera using prepacked KP-SIL silica gel SNAP cartridges (50  $\mu$ m). Thin layer chromatography was run on aluminium-backed plates precoated with silica gel 60F<sub>254</sub> (Merck) and spots were visualized with a UV lamp or stained with ninhydrin. Spectra were recorded on a 400, 500, or 600 MHz Bruker NMR spectrometer, and chemical shifts are reported in parts per million and corrected relative to the solvent as internal standard (CDCl<sub>3</sub>,  $\delta$  7.26). Multiplicity is reported as follows: s, singlet; d, doublet; t, triplet; m, multiplet; br s, broad singlet. IR was run on a Nicolet iS5 from Thermo Fisher mounted with an iD5 ATR. Optical rotation was measured on an Autopol V automatic polarimeter (Rudolph Research Analytical) using the sodium D line at 589 nm.

Peptides were synthesized on a Biotage Initiator + Alstra microwave assisted peptide synthesizer. Reactions requiring microwave heating were performed using a CEM Discover SP microwave. Peptides were purified on a reverse-phase Dionex high performance liquid chromatography (HPLC) system equipped with Dionex P680 pumps and a Dionex UVD170U UV-vis detector (monitoring at 214 nm and 280 nm), using a Phenomenex Gemini, C18, 5  $\mu$ m, 250  $\times$  21.2 mm column. Gradients were run using a solvent system consisting of A (H<sub>2</sub>O + 0.1% TFA) and B (H<sub>2</sub>O + 0.1% TFA), and collected fractions were lyophilised on a Christ Alpha 2-4 LO plus freeze dryer.

Pure peptides were analyzed on a Shimadzu reverse-phase HPLC (RP-HPLC) system equipped with Shimadzu LC-20AT pumps, a Shimadzu SIL-20A autosampler and a Shimadzu SPD-20A UV-vis detector (monitoring at 214 nm and 280 nm) using a Phenomenex, Aeris, 5  $\mu$ m, peptide XB-C18, 150  $\times$  4.6 mm column at a flow rate of 1 mL/min. RP-HPLC gradients were run using a solvent system consisting of solution A (5% acetonitrile [MeCN] in H<sub>2</sub>O + 0.1% TFA) and B (5% H<sub>2</sub>O in MeCN + 0.1% TFA). Two gradients were used to characterize each peptide; a gradient from 0% to 100% solution B over 20 minutes and either a 50 minutes gradient from 0%–100% solution B or a 25 minutes gradient from 0–50% solution B, respectively. Analytical RP-HPLC data is reported as column retention time ( $t_R$ ) in minutes (min). Low resolution mass spectrometry (LRMS) was performed on a Thermo Scientific LCQ Fleet quadrupole mass spectrometer using positive mode electrospray ionization (ESI<sup>+</sup>). High resolution mass spectrometry (HRMS) was performed on a Bruker

microTOF-Q II (ESI<sup>+</sup>). HRMS data are reported as mass to charge ratio ( $m/z$ ) = observed / MW.

Peptide content was analyzed on a Nanodrop 2000c using UV absorption of peptides at 280 nm.

## 2.2 | Peptide synthesis

Peptides were synthesized on 0.1 mmol scale using ChemMatrix Rink Amide Resin (0.47 mmol/g) (Biotage). Couplings were performed using 4 equivalents Fmoc-protected amino acid, 4 equivalents HCTU and 4 equivalents diisopropylethylamine (DIPEA) in DMF (3 mL). Coupling of standard Fmoc-protected amino acids was carried out for 10 minutes at 75 °C followed by 4 × 45 seconds washes. Arginine was double coupled; 60 minutes at room temperature followed by 5 minutes at 75 °C and repeated with fresh reagents followed by washing. Histidine and cysteine were coupled at room temperature for 5 minutes followed by 50 °C for 5 minutes and washes. For coupling of unnatural amino acids only 2 equivalents of reagents were used.

Deprotection was carried out in 20% piperidine in DMF + 0.1 M Oxyma Pure (4.5 mL) for 30s and then 3 minutes at 75 °C followed by washing. Following coupling of Fmoc-Asp(tBu)-OH all Fmoc-deprotections were carried out at room temperature for 3 minutes and then 10 minutes followed by washing. N-terminal acetylation was performed using 1 mL 5 M acetic anhydride in DMF and 2.5 mL 2 M DIPEA in NMP for 10 minutes at room temperature.

Test cleavages were performed in a cleavage cocktail (1 mL) of 95% trifluoroacetic acid (TFA), 2.5% water (H<sub>2</sub>O) and 2.5% triisopropylsilane (TIS) for 30 minutes at room temperature and the cleavage cocktail was evaporated using a stream of nitrogen. The peptide was precipitated from solution with ice-cold diethyl ether (Et<sub>2</sub>O), centrifuged at 4500 rpm for 5 minutes and the precipitate was dissolved in 50/50 MeCN/H<sub>2</sub>O, centrifuged at 4500 rpm for 5 minutes and run using LC-MS and/or analytical HPLC.

Peptides containing cysteines were cleaved in a cleavage cocktail (10 mL) of 94% TFA, 2.5% 1,2-ethanedithiol (EDT), 2.5% H<sub>2</sub>O and 1% TIS. Peptides without cysteines were cleaved in a cleavage cocktail (10 mL) of 95% TFA, 2.5% H<sub>2</sub>O and 2.5% TIS. The resin was stirred for 3 hours at room temperature and the cleavage cocktail was evaporated using a stream of nitrogen. The peptides were precipitated from solution with ice-cold Et<sub>2</sub>O, centrifuged at 4500 rpm for 5 minutes and the precipitate washed with ice cold Et<sub>2</sub>O. The peptide was dissolved in H<sub>2</sub>O/MeCN + a few drops of glacial acetic acid and lyophilised overnight.

### 2.2.1 | Synthesis of the native $\mu$ -KIIIA peptides 1 and 2

The linear peptide was synthesized, cleaved from resin and purified as described above. Peptide content was determined and the peptide was oxidized at a concentration of 20  $\mu$ M to avoid polymerization. The peptide was oxidized using air oxidation in a 0.1 M ammonium carbonate (NH<sub>4</sub>HCO<sub>3</sub>) buffer at pH 7.5, which was degassed using N<sub>2</sub> for 1 hour

prior to use. The reaction was monitored using LC-MS, and typically showed full conversion after 2-3 hours. The solution was then freeze dried and the residual solid taken into MeOH, which was removed in vacuo at 40 °C to remove most of the NH<sub>4</sub>HCO<sub>3</sub>-salt. The remaining solid was then dissolved in a mixture of H<sub>2</sub>O/MeCN and purified as specified above yielding both the major and the minor folded isomers.

### 2.2.2 | Synthesis of the hydrocarbon stapled peptides 3, 4, 5 and 6 using ring closing-metathesis

The linear peptide was synthesized using solid phase peptide synthesis (SPPS) as described above. The resin was suspended in dry dichloroethane (DCE) (0.025 M) and 20 mol% Grubbs first catalyst was added. The reaction was shaken for 2 hours at room temperature excluding light. Following 3 × 1 minute dichloromethane (DCM) washes the procedure was repeated. If full conversion had not been attained the procedure was repeated in the microwave at 40 °C. After the final RCM the resin was thoroughly washed (3 × 1 minute DMF, 3 × 1 minute isopropanol (iPrOH, 3 × 1 minute DCM) before resin cleavage/global deprotection and purification as described above.

### 2.2.3 | Synthesis of the reduced hydrocarbon stapled peptide 5

Resin containing hydrocarbon stapled peptide was swollen in *N*-methyl-2-pyrrolidone (NMP) for 20 minutes, the solvent removed and a mixture of triisopropylbenzenesulfonyl hydrazide (TPSH) (270 mg, 0.9 mmol, 9 eq.) and piperidine (180  $\mu$ L, 1.8 mmol, 18 eq.) in 1 mL NMP was added. The resin was kept at 48 °C for 2 hours. The procedure was repeated 4-5 times. The resin was then thoroughly washed (3 × 1 minute DMF, 3 × 1 minute iPrOH, 3 × 1 minute DCM) before resin cleavage/global deprotection and purification as described above.

### 2.2.4 | Synthesis of the 1,4-triazole constrained peptide 7

The linear peptide was synthesized using the azide- and alkyne  $\alpha$ -methyl amino acids **S8** and **S9** (see synthesis below) and cleaved from resin as described above. The crude peptide was then dissolved in pure, degassed H<sub>2</sub>O at 1 mg/mL concentration and 1 eq. sodium ascorbate (NaAsc), 1 eq. copper(II) sulfate pentahydrate (CuSO<sub>4</sub>·5H<sub>2</sub>O) and 8 eq. DIPEA were added. The solution was stirred at room temperature overnight. The reaction was then lyophilised and purified as described above.

### 2.2.5 | Synthesis of the 1,5-triazole constrained peptide 8

The linear peptide was synthesized using the azide- and alkyne  $\alpha$ -methyl amino acids **S8** and **S9** (see synthesis below). The resin was

dried for 24 hours in a desiccator before being taken into 2 mL dry DMF and degassed for 20 minutes using argon gas. A 20 mol% [Cp\*RuCl(COD)] was added and the solution was degassed for a further 10 minutes. The resin was then reacted in a microwave at 60 °C for 6 hours. The resin was washed thoroughly (3 × 1 minute DMF, 3 × 1 minute iPrOH, 3 × 1 minute DCM) and cleaved/globally deprotected and purified as described above.

## 2.2.6 | Synthesis of the lactam constrained peptide 9

The linear peptide was synthesized using SPPS as described above, except that for Asp3 the amino acid Fmoc-Asp(2-O-Ph<sup>i</sup>Pr)-OH was used and for Lys7 the amino acid Fmoc-Lys(Mmt)-OH was used. The resin was swollen in DCM and washed with a solution of 2% TFA in DCM until the wash solution did not show a strong yellow color. The resin was then washed thoroughly (3 × 1 minute DMF, 3 × 1 minute iPrOH, 3 × 1 minute DCM). The lactam was coupled using 1 eq. HCTU and 3 eq. DIPEA for 2 hours at room temperature and the coupling procedure was repeated using fresh reagents. The resin was washed thoroughly (3 × 1 minute DMF, 3 × 1 minute iPrOH, 3 × 1 minute DCM) and cleaved/globally deprotected and purified as described above.

## 2.3 | Circular dichroism

Circular dichroism was performed on a Jasco J-810 spectropolarimeter at 20 °C. Concentration was determined on a Nanodrop and samples of 50 μM and 100 μM were made in pure H<sub>2</sub>O with a maximum of 1% MeCN (final concentration) added for solubility. Before running CD the concentrations were checked again. Each sample was run at two different concentrations (50 μM and 100 μM) with 0.2 nm increments, 10 nm/step and 2 seconds response time. Both concentrations were compared to ensure that no dimerization/oligomerisation had occurred. A control sample containing pure H<sub>2</sub>O was subtracted and the graph smoothed.

The raw data was corrected to give mean residue ellipticity (MRE) according to the following equation:

$$\text{MRE} = (E, 10^6) / l, c, n$$

Where E is ellipticity in mdeg; l is pathlength in mm; c is peptide concentration in μM; n is number of amide bonds in the peptide.

## 2.4 | Patch-clamp assay

Human embryonic kidney (HEK-293) cells expressing human Na<sub>v</sub>1.4 (SB Drug Discovery, Glasgow, UK) were cultured in minimum essential media (MEM) medium with heat-inactivated Foetal Bovine Serum (FBS) (10%) glutamine (2 mM) penicillin/streptomycin (50 units/mL),

blasticidin (2 μg/mL) and geneticin 418 (0.6 mg/mL). Cells were grown in a humidified 5% CO<sub>2</sub> incubator at 37 °C, grown to 70/80% confluence and passaged every 3 to 4 days using TrypLE express. For electrophysiology experiments cells were dissociated with TrypLE then resuspended in Ex-Cell ACF CHO medium and allowed to recover with stirring for 45 minutes on the Q-patch.

Whole cell patch clamp experiments were performed on a QPatch-16 automated electrophysiology platform (Sophion, Ballerup, Denmark) using 16 channel QPlates. The extracellular solution (ECS) contained 145 mM NaCl, 4 mM KCl, 1 mM MgCl<sub>2</sub>, 2 mM CaCl<sub>2</sub>, 10 mM HEPES and 10 mM glucose, pH 7.4. The intracellular solution (ICS) contained 140 mM CsF, 1 mM EGTA, 10 mM HEPES, 5 mM CsOH and 10 mM NaCl, pH 7.25. The holding potential was −90 mV and channels were activated with a depolarizing step to 0 mV for 10 ms.

Compounds were added to the cells in a cumulative fashion during and for each cell, tetrodotoxin (TTX, 1 μM) was applied after the compound applications of μ-conotoxin KIIIA or mimetics/controls to act as a positive control as Na<sub>v</sub>1.4 and Na<sub>v</sub>1.6 are TTX sensitive.

A baseline correction was applied to the patch clamp data generated on the QPatch. This data was exported and analyzed using GraphPad Prism 8.0 for Windows (San Diego, California). Nonlinear regression was performed and a 4-parameter logistic fit was used with the bottom of the curve constrained to 0. This fit was used to calculate the IC<sub>50</sub> and Hill Coefficient values. For minor isomer 2 at Na<sub>v</sub>1.6 the maximal block was not sufficient to generate IC<sub>50</sub> or Hill Coefficient values.

## 2.5 | NMR assignment of stapled peptide alkene isomers 3, 4 and 6

Samples were dissolved at between 0.2 and 1 mM in H<sub>2</sub>O with 5% D<sub>2</sub>O and 250 p.p.m. TSP as a reference and 600 μL placed in a 5 mM NMR tube (Wilmad 535-PP-7). All experiments were recorded using a Bruker AVIII HD spectrometer operating at 599.87 MHz for <sup>1</sup>H using a TCI cryoprobe. For assignment and structure determination, <sup>1</sup>H-<sup>1</sup>H TOCSY, DQF-COSY, <sup>1</sup>H-<sup>13</sup>C HSQC and <sup>1</sup>H-<sup>1</sup>H NOESY spectra with zero quantum suppression were recorded at 278 K. The NOESY data for structure determination were collected at three different mixing times (80, 200, 300 ms).<sup>[25]</sup> The spectra were assigned using CCPN analysis 2.4 and the structures calculated with ARIA2.3/CNS1.2.<sup>[26,27]</sup> From 100 structures calculated in the final iteration, the 20 lowest energy were refined in explicit water and the structure with the lowest overall energy used in further analysis.<sup>[28]</sup>

## 3 | RESULTS AND DISCUSSION

### 3.1 | Design and synthesis of peptidomimetics

Synthesis of native μ-KIIIA and stapled KIIIA-mimetics was achieved with ChemMatrix Rink amide resin using standard Fmoc-based solid

phase peptide synthesis (SPPS). The native linear  $\mu$ -KIIIA peptide was cleaved from the resin and purified before being oxidized to yield a complex mixture (Scheme 1) from which the major isomer (**1**, eluting first [see insert in scheme]) and the minor isomer (**2**, eluting second) could be isolated. Disulfide connectivities of these two isomers have previously been reported.<sup>[29]</sup> The two native isomers were tested to ensure biological efficacy (*vide infra*).

As the published NMR structure of the native  $\mu$ -KIIIA (isomer **1**) is  $\alpha$ -helical<sup>[29]</sup> we replaced the disulfide bond network with synthetic staples which have been shown previously to stabilize  $\alpha$ -helical structures by bridging either one ( $i$  to  $i + 4$ ) or two helical turns ( $i$  to  $i + 7$ ) (Figure 1).<sup>[30]</sup> A previous study on  $\mu$ -KIIIA found six residues to be important for biological activity: K7, W8, R10, D11, H12 and R14.<sup>[31]</sup> We based the produced mimetics on this truncated 6-residue core placing unnatural amino acids for stapling at the  $i$  and  $i + 4$ , or  $i$  and  $i + 7$ , positions (Figure 1). We synthesized four different  $i, i + 4$  staples, three  $i, i + 7$  staples and three controls (Figure 1).

We employed the hydrocarbon-stapling (HCS) strategy developed by Verdine and co-workers<sup>[32]</sup> as the unnatural amino acids required are commercially available.<sup>[33]</sup> The linear peptide **13** incorporating (R)-N-Fmoc- $\alpha$ -(7-octenyl) alanine at position  $i$  and (S)-N-Fmoc- $\alpha$ -(4-pentenyl)alanine at position  $i + 7$  was prepared using standard Fmoc/<sup>t</sup>Bu SPPS methods. Linear peptide **14**, incorporating two (S)-N-Fmoc- $\alpha$ -(4-pentenyl)alanine residues in the  $i$  and  $i + 4$  positions (Scheme 2C) was also prepared to provide the shorter conformational constraint. Ring-closing metathesis (RCM) was achieved using 20 mol% Grubbs first catalyst at room temperature followed by resin cleavage, global deprotection, and RP-HPLC purification. Applied to **13**, this resulted in both the *trans* (**3**) and *cis* (**4**)  $i, i + 7$  stapled peptide isomers (Scheme 2A) being isolated, whereas **14** yielded only the *cis*  $i, i + 4$  stapled peptide isomer (**6**) (Scheme 2C). We also produced the peptide incorporating (R)-N-Fmoc- $\alpha$ -(7-octenyl)alanine at position  $i$  and (S)-N-Fmoc- $\alpha$ -(4-pentenyl)alanine at position  $i + 7$ , but in this case no RCM reaction was observed at room temperature, and heating produced a complex mixture including epimers (detected by LC-MS analysis of a cleaved sample). The configurational isomerism for **3**, **4** and **6** was

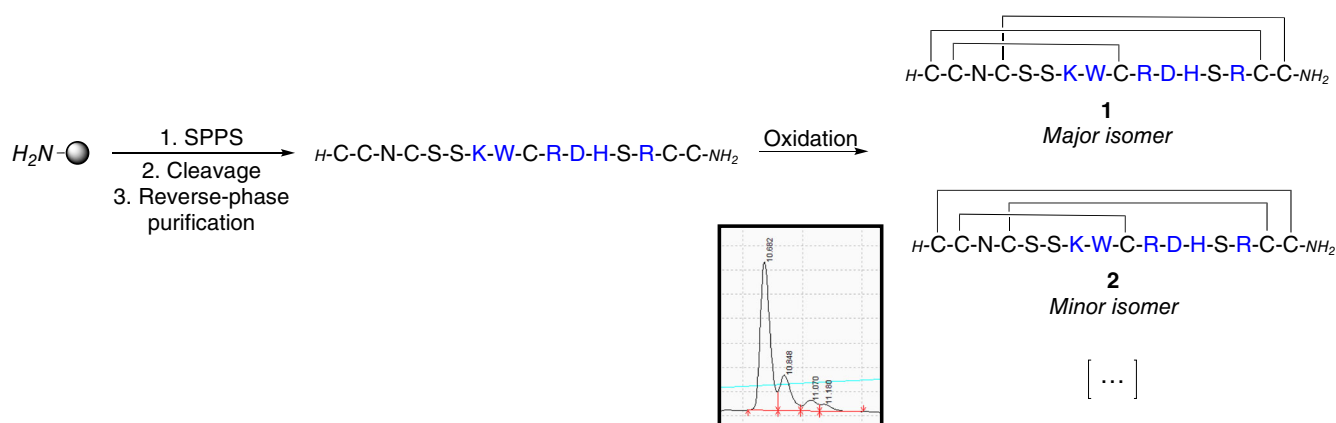
confirmed by homonuclear decoupling <sup>1</sup>H NMR experiments (Figures S2 to S4 in SI).

Furthermore, as RCM of peptide **13** produced both the *cis* and *trans* isomers **3** and **4** and to investigate further the effect of the carbon-carbon double bond on the effectiveness of the hydrocarbon constraint, we also produced the reduced  $i, i + 7$  staple **5**. After RCM to produce peptides **3** and **4**, the double bond was reduced on resin, using triisopropylbenzenesulfonyl hydrazide under basic conditions and elevated temperature to provide saturated stapled peptide **5** (Scheme 2B).<sup>[34]</sup>

We next wanted to explore the effectiveness of 1,4- and 1,5-triazole moieties as conformational constraints and surrogates for the alkene isomers. To make the closest comparison with the  $\alpha$ -methyl substituted HCS mimetics, two  $\alpha$ -methyl  $\alpha$ -amino acids were synthesized; alkyne **S8** and azide **S9** (Scheme S1) based on our previously published methodology.<sup>[35]</sup> These amino acids were used to synthesize linear peptide **15**, and the peptide then cleaved from the solid support. Macrocyclisation of **15** was achieved using a Cu(I)-catalyzed azide-alkyne cycloaddition (CuAAC) in solution (Scheme 2D) resulting in the  $i, i + 4$  stapled 1,4-disubstituted 1,2,3-triazole (**7**). We also applied Ru(I)-catalyzed azide-alkyne cycloaddition (RuAAC) on resin (Scheme 2E) to yield the 1,5-disubstituted 1,2,3-triazole  $i, i + 4$  stapled mimetic **8**.

To compare our mimetics with the most potent  $\mu$ -KIIIA mimetic reported by Khoo *et al.*,<sup>[23]</sup> we synthesized the lactam analogue **9** using a modified method, as the authors had used Boc-chemistry. To make a direct comparison with the reported mimetic, we prepared this analogue without  $\alpha$ -methyl amino acid substitution. We employed an orthogonal protection strategy, using 2-phenyl isopropyl ester (O-2-PhIPr) protected Asp3, and 4-methoxytrityl (Mmt) protected Lys7, that were simultaneously removed in 2% trifluoroacetic acid (TFA) in dichloromethane. Macro-lactamisation was achieved on resin (Scheme 2F) to provide the stapled peptide, which was cleaved and purified by RP-HPLC.

Finally, we synthesized the three linear peptide controls **10**, **11** and **12** (Figure 1). Peptides **10** and **11** are alanine analogues of the  $i$ ,



**SCHEME 1** Synthesis of native  $\mu$ -KIIIA. The peptide was synthesized using standard SPPS protocols cleaved and purified before being oxidized to yield several isomers of which two, **1** and **2**, could be isolated. Insert: HPLC chromatogram showing the complex oxidation mixture



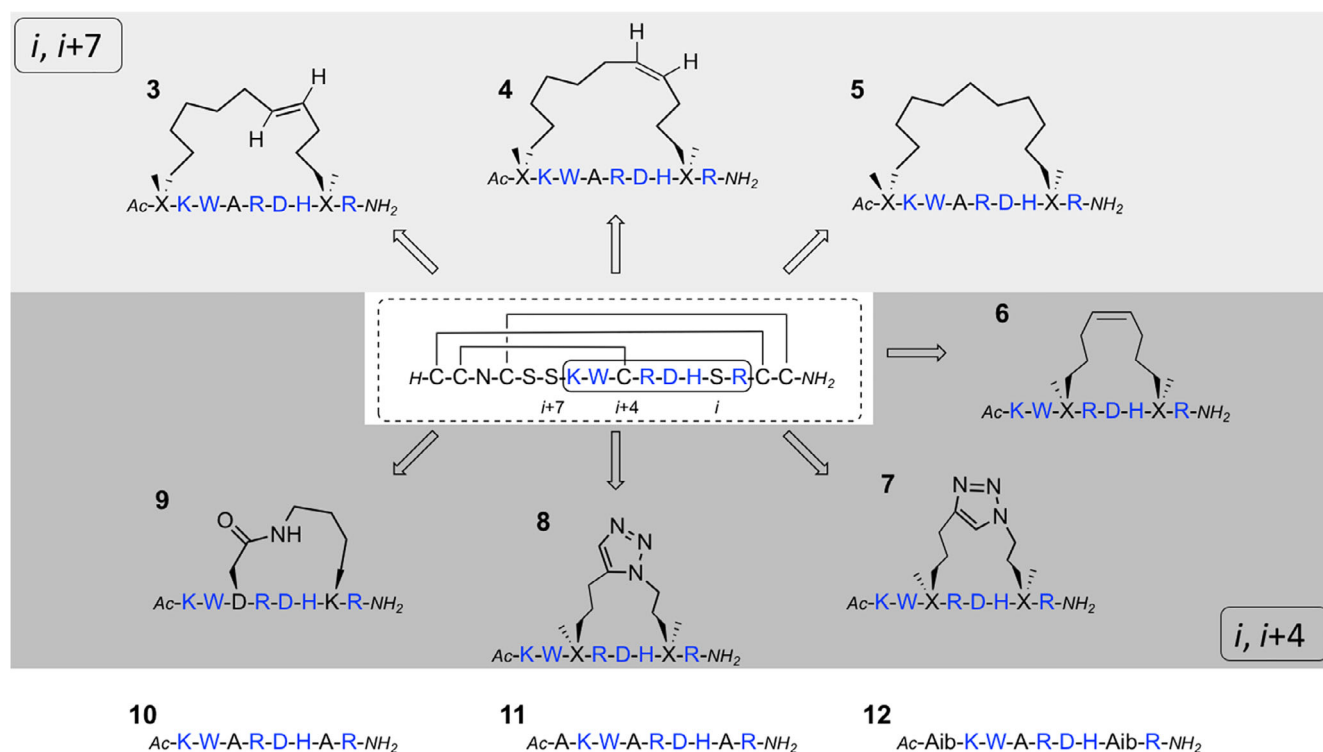


**FIGURE 1** The three  $i, i+7$  mimetics (3-5), the four  $i, i+4$  mimetics (6-9) and the three control mimetics (10-12) all based on the native  $\mu$ -KIIIA

$i+4$  and  $i, i+7$  stapled peptides, respectively. Peptide 12 incorporates Aib residues to investigate the effect of the  $\alpha$ -methyl group in the  $i, i+7$  peptidomimetics.

### 3.2 | Patch clamp evaluation of $\mu$ -KIIIA-mimetics in hNav1.4 and hNav1.6 expressing HEK cells

The two native isomers (1-2), the stapled mimetics (3-9) and the controls (10-12) were evaluated in a patch-clamp assay using human embryonic kidney (HEK) cells expressing the human Nav1.4 (hNav1.4) or Nav1.6 (hNav1.6) channels (Figure 2).

The major native isomer 1 gave an  $\text{IC}_{50}$  of 200 nM against hNav1.4 and  $\text{IC}_{50}$  of 600 nM against hNav1.6, whereas the minor isomer 2 was  $\sim 30$  times (hNav1.4) and markedly (hNav1.6) less active than the major isomer. Interestingly, the three  $i, i+7$  mimetics 3-5 were the only mimetics to show inhibition of the two channels; in hNav1.4 the trans 3 and reduced 5 staples showed almost equipotent inhibition, with the trans staple 3 having a slightly better  $\text{IC}_{50}$  of 36.4  $\mu\text{M}$ , compared to 38.9  $\mu\text{M}$  for the reduced staple 5 (Table 1). The cis stapled mimetic 4 was 3.9-fold less active than the trans staple 3 with an  $\text{IC}_{50}$  of 140.9  $\mu\text{M}$ . Against hNav1.6 channels, however, only the reduced staple 5 showed low micromolar inhibition with an  $\text{IC}_{50}$  of 76.23  $\mu\text{M}$ , whereas the trans 3 and cis 4 staples were 1.4- and 3.8-fold less potent, respectively. None of the  $i, i+4$  mimetics 6-9 or the controls 10-12 showed any inhibition in either channel type (Figure S1 in the SI), indicating that the longer  $i, i+7$  staples seem to be required to provide a bioactive conformation.

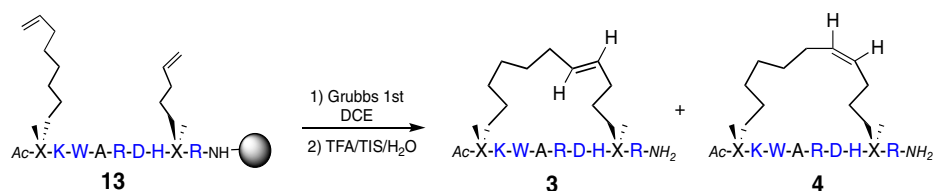
### 3.3 | Circular dichroism of the $\mu$ -KIIIA-mimetics

The circular dichroism (CD) spectra of each of the peptides in water were acquired to evaluate the degree of  $\alpha$ -helicity induced by the different conformational constraints to that of the linear controls (Figure 3). All peptides were run at two concentrations (50 and 100  $\mu\text{M}$ ) to ensure the results were independent of concentration (data for 100  $\mu\text{M}$  shown in Figure 3), and then corrected to mean residue ellipticity (MRE; see SI).

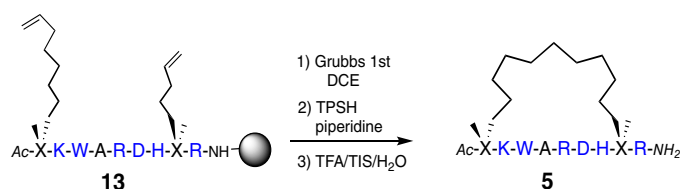
The CD data for the three  $i, i+7$  HCS mimetics (3-5) and the two linear  $i, i+7$  controls (11 and 12) are presented in Figure 3A. CD data for the four  $i, i+4$  stapled mimetics (6-9) and the linear  $i, i+4$  control (10) are shown in Figure 3B. We examined the  $\alpha$ -helicity of the compounds based on the three extrema; the maxima at 190 nm and the two minima at 208 nm and 222 nm, which are known to be indicators of  $\alpha$ -helical structure.<sup>[36]</sup> For the  $i, i+7$  staples there was a striking pattern; the trans-alkene hydrocarbon mimetic 3 (dark green) showed most  $\alpha$ -helical character, followed by the reduced hydrocarbon-staple 5 (purple), with the cis-alkene hydrocarbon mimetic 4 (dark blue) showing the least  $\alpha$ -helical character. Of the  $i, i+4$  mimetics, the cis-alkene hydrocarbon mimetic 6 (red), showed the most  $\alpha$ -helical character, followed by the lactam-stapled mimetic 9 (light green). Interestingly, the 1,5-triazole stapled-mimetic 8 (light blue), showed good  $\alpha$ -helical character, whereas the CD curve from the 1,4-triazole stapled-mimetic 7 (orange) indicated a random coil conformation. We have previously shown that a 1,5-triazole bridge is a better disulfide surrogate than the 1,4-triazole analogue.<sup>[37,38]</sup> The current data suggests that a 1,5-triazole bridge provides a similar type of constraint as a cis- $i, i+4$  hydrocarbon alkene staple and can effectively promote  $\alpha$ -helical

**SCHEME 2** Synthesis of (A) *trans* (**3**) and *cis* (**4**) *i, i + 7* HCS mimetics; (B) reduced *i, i + 7* HCS mimetic (**5**); (C) *i, i + 4* *cis* HCS mimetic (**6**); (D) *i, i + 4* 1,4-disubstituted 1,2,3-triazole mimetic (**7**); (E) *i, i + 4* 1,5-disubstituted 1,2,3-triazole mimetic (**8**); (F) *i, i + 4* lactam mimetic (**9**). TFA, trifluoroacetic acid; TIS, triisopropylsilane; DCE, dichloroethane; TPSH, 2,4,6-triisopropylbenzenesulfonyl hydrazide; NaAsc, sodium ascorbate; DIPEA, *N,N*-diisopropylethylamine; HCTU, *O*-(1*H*-6-chlorobenzotriazole-1-yl)-1,1,3,3-tetramethyluronium hexafluorophosphate

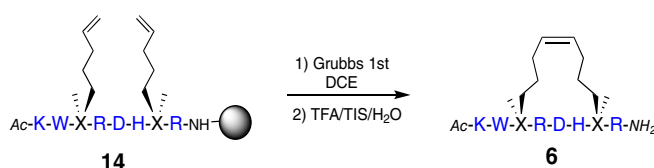
**A) *i, i + 7* hydrocarbon staples**



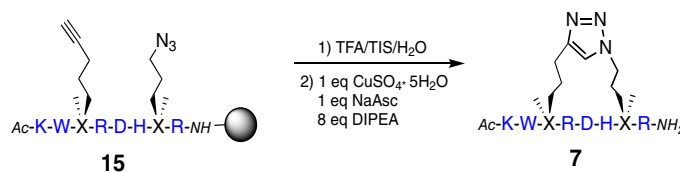
**B) *i, i + 7* reduced hydrocarbon staple**



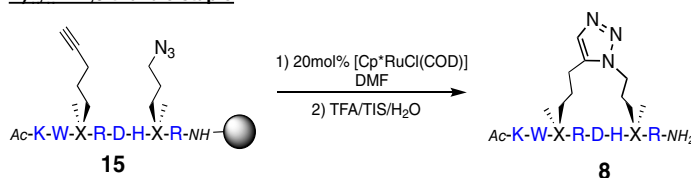
**C) *i, i + 4* hydrocarbon staple**



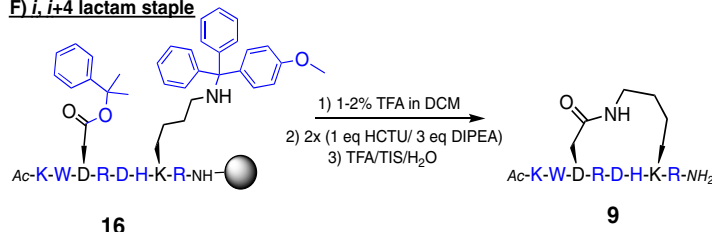
**D) *i, i + 4* 1,4-triazole staple**



**E) *i, i + 4* 1,5-triazole staple**



**F) *i, i + 4* lactam staple**



character in a peptide. The linear peptide controls **10**, **11** and **12** all show significantly less  $\alpha$ -helical character than the stapled peptidomimetics.

The longer *i, i + 7* staples seem to be required to provide a bioactive conformation and biological activity against *hNav1.4* and *hNav1.6*. However, there appears to be little correlation between the CD peptide helicity of the *i, i + 4* constrained analogues and bioactivity. Thus, we decided to explore the secondary structure of the three most  $\alpha$ -helical compounds (**3**, **5** and **6**) according to CD using solution-phase NMR spectroscopy.

### 3.4 | Conformational evaluation of mimetics **3** and **5** by NMR

NMR spectroscopy has played a key role in providing the structures of peptide toxins and facilitating structure activity relationship studies.<sup>[39]</sup> The use of NMR/X-ray structural methods provides an accurate atomistic description of a peptide structure; however they require the computational description of nonnatural linkages and

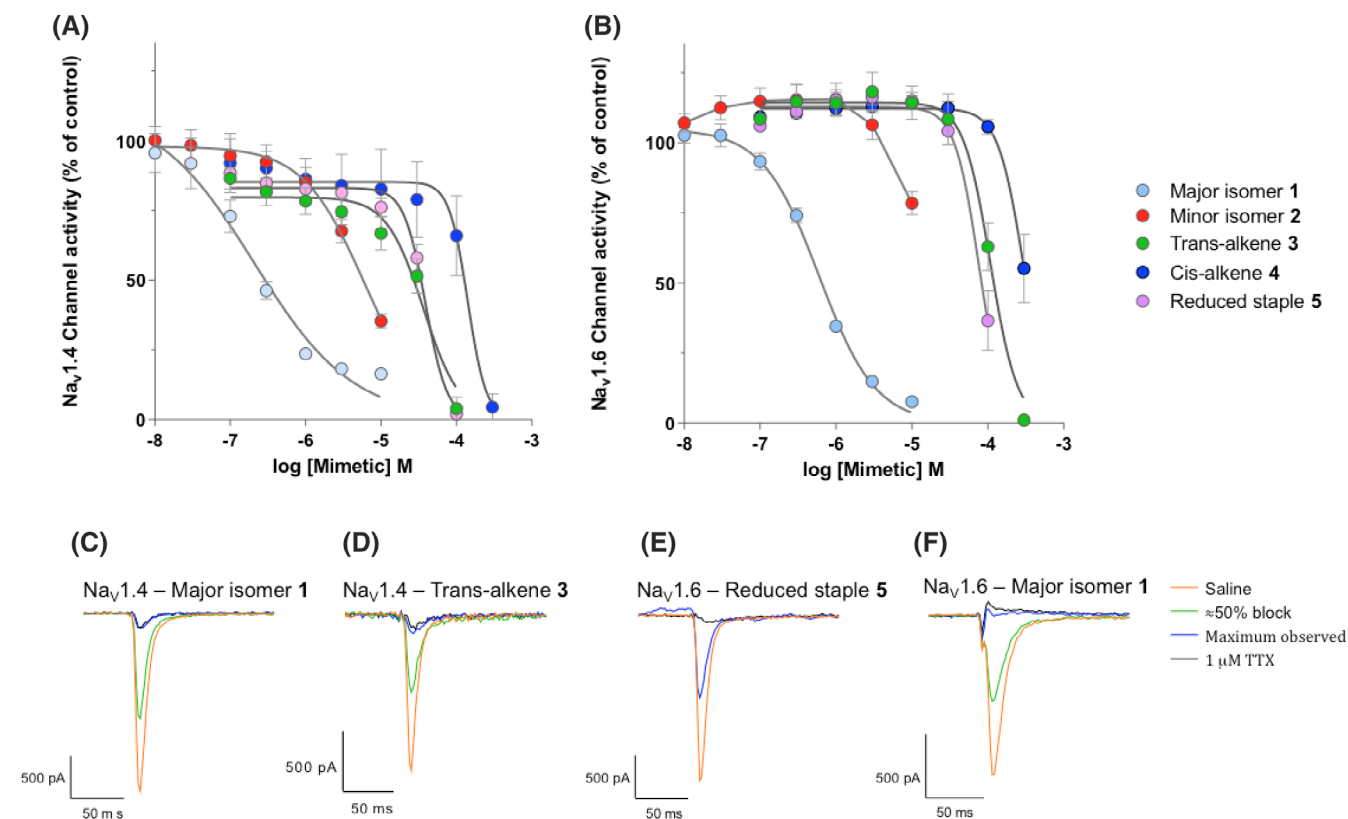


**FIGURE 2** Patch-clamp testing of the native major 1 and minor 2  $\mu$ -KIIIA, and the active and partially active mimetics 3–5. (A) Testing of compounds 1–5 in HEK293 cells expressing the human Na<sub>v</sub>1.4 channel ( $n = 9$ –24). (B) Testing of compounds 1–5 in HEK293 cells expressing the human Na<sub>v</sub>1.6 channel ( $n = 7$ –27). (C–F) Patch clamp trace data from Na<sub>v</sub>1.4 (C, D) and Na<sub>v</sub>1.6 (E, F) cells, with the green and blue lines representing the following (C)  $\approx 50\%$  block at  $0.3 \mu\text{M}$ , maximum observed block at  $10 \mu\text{M}$  (D)  $\approx 50\%$  block at  $3 \mu\text{M}$ , maximum observed block at  $100 \mu\text{M}$  (E) maximum observed block at  $100 \mu\text{M}$  (F)  $\approx 50\%$  block at  $1 \mu\text{M}$ , maximum observed block at  $10 \mu\text{M}$

**TABLE 1** Comparison of the patch-clamp data for the two native m-KIIIA isomers, major (1) and minor (2), as well as the three most bioactive mimetics: trans-alkene (3), cis-alkene (4) and reduced-staple (5)

Mimetic	Na <sub>v</sub> 1.4			Na <sub>v</sub> 1.6		
	IC <sub>50</sub> ( $\mu\text{M}$ )	Hill coefficient	Maximal block (%) and mimetic concentration at which this block occurred	IC <sub>50</sub> ( $\mu\text{M}$ )	Hill coefficient	Maximal block (%) and mimetic concentration at which this block occurred
Major $\mu$ -KIIIA (1)	0.20	-0.66	84% ( $10 \mu\text{M}$ )	0.60	-1.17	92% ( $10 \mu\text{M}$ )
Minor $\mu$ -KIIIA (2)	6.02	-1.06	65% ( $10 \mu\text{M}$ )	*	*	22% ( $10 \mu\text{M}$ )
Trans-alkene (3)	36.4	-1.78	96% ( $100 \mu\text{M}$ )	108.0–2.45	99% ( $300 \mu\text{M}$ )	
Cis-alkene (4)	140.9	-3.53	96% ( $300 \mu\text{M}$ )	296.3	-2.57	45% ( $300 \mu\text{M}$ )
Reduced-staple (5)	38.9	-3.03	98% ( $100 \mu\text{M}$ )	76.23	-2.73	64% ( $100 \mu\text{M}$ )

Note: The compounds were tested in HEK293 cells expressing either the human Na<sub>v</sub>1.4 or the human Na<sub>v</sub>1.6 ( $n = 7$ –24). Data were fitted to a sigmoidal dose response-curve and used to calculate IC<sub>50</sub> and Hill Coefficient values. \* denotes compounds where a curve fit was not possible.

only NMR spectroscopy can provide information concerning solution structural dynamics. Therefore, for the most active all-hydrocarbon mimetics 3 and 5 we produced modified CNS topology/parameter descriptions (Figures S8 and S9), which in conjunction with NOE-derived distance restraints, were used to compute solution structures of these mimetics. Near complete resonance assignment was achieved despite the degeneracy of the alkane linker signals and the calculated structures were well

converged with good agreement with the experimental data (Tables S1 and S2).

Peptidomimetics 3 and 5 are  $\alpha$ -helical throughout the sequence bounded by the linker residues and are structurally similar to each other ( $0.52 \text{ \AA}$  backbone RMSD between the representative structures), consistent with the similar bioactivity observed for each mimetic against hNa<sub>v</sub>1.4 (Figure 4A). Comparison of each of the mimetics with the structure of the native toxin (Figure 4B,C) shows that the amino acids



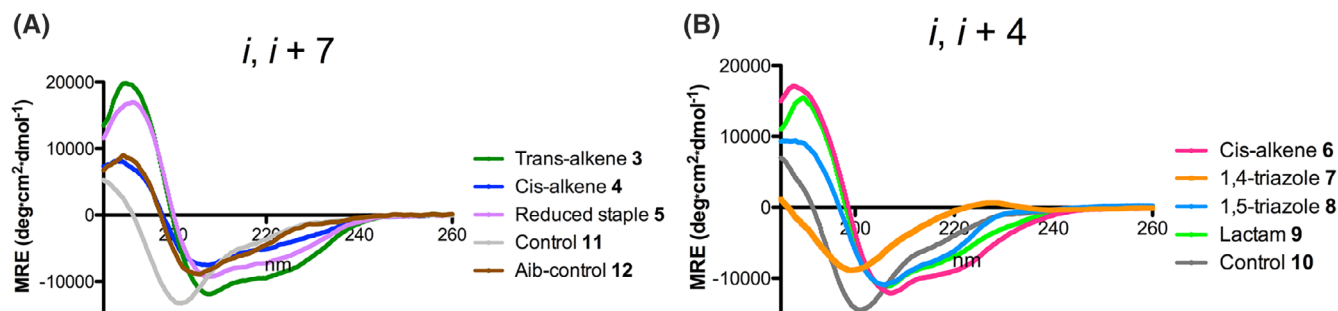
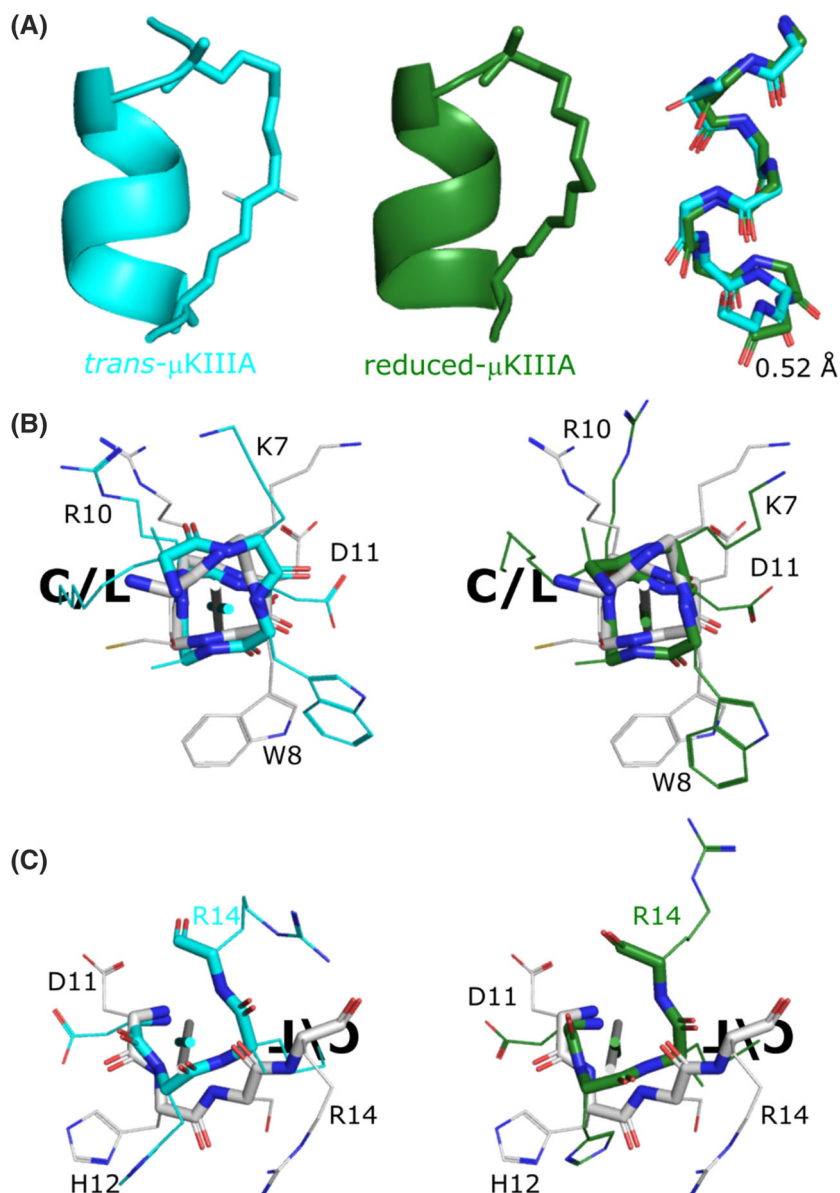


**FIGURE 3** Circular dichroism of the 10 mimetics and controls. (A) Circular dichroism data of the three  $i, i + 7$  mimetics **3–5** and the two  $i, i + 7$  controls **11** and **12**. (B) Circular dichroism data of the four  $i, i + 4$  mimetics **6–9** and the  $i, i + 4$  control **10**. Data are corrected for mean residue ellipticity and recorded in water containing maximum 1% acetonitrile for solubility

**FIGURE 4** Structures of  $\mu$ -KIIIA mimetics determined by NMR spectroscopy. (A) Both the trans- (**3**) and reduced- (**5**) structures exhibit a helical core and are structurally similar (0.52 Å backbone RMSD). (B) The N-terminal residues of both mimetics exhibit close structural similarity to the native toxin (PDB:2LXG, gray) and project similar functional groups along similar vectors. (C) The C-terminal half of the mimetics continue in a helical arrangement past the stapled linker residue, whereas the native structure uncoils to connect to the Cys-rich core producing significant differences in structure around Arg14. Backbone atoms are shown as sticks and sidechains as lines with N and O colored blue and red, respectively. In B & C, the views are related by a 180° rotation around the page vertical and the helix axis of each structure is shown as a thin cylinder and the location of the Cys-rich core/stapled linker region indicated as C/L



essential for bioactivity, namely K7, W8, R10, and D11,<sup>[31]</sup> are positioned similarly. The side chain of W8 in both mimetics is comparatively unconstrained compared to the native toxin, and more so in mimetic **3**,

which may explain the difference in activity at the two different  $\text{Na}_V$ -channels. In the native  $\mu$ -KIIIA, W8 interacts with the Cys-rich core, while in the mimetics the linkers are too distant to contact it.

A feature of the native structure is that, beyond H12, the helix unwinds to make the turn into the Cys-rich core, whereas the mimetics remain helical throughout, and thus do not effectively mimic the C-terminal end of the native structure. The deviation is clearest in the backbone conformation of R14, which in the mimetic structures is firmly within a helical turn controlled by the adjacent  $\alpha,\alpha$ -disubstituted nonnatural amino acid, whereas in the native structure the helix is essentially uncoiled (Figure 4C). Replacement of the terminal Arg has previously been shown to greatly reduce the binding of native  $\mu$ -KIIIA to  $\text{Na}_V1.4$  and reduce the  $k_{\text{on}}$  for binding to the receptor.<sup>[31]</sup> It is possible that the inaccurate placement of this residue in the mimetics could be responsible for their lower affinity.

We also attempted to determine the structure of  $i,i + 4$  stapled mimetic **6**, which gave a similar CD spectrum, indicative of a high  $\alpha$ -helical content, to that of the  $i,i + 7$  mimetic **3**, but in contrast to mimetic **3** did not show any bioactivity in the patch-clamp assays. The NOE crosspeaks for the  $i,i + 7$  mimetics, for example, **5**, are well resolved (Figure S12A) whereas the crosspeaks for mimetic **6** are broadened (Figure S12B), indicating that the staple in mimetic **6** does not stabilize the structure in a single conformation. As CD and NMR are sensitive to structural changes on different timescales<sup>[40]</sup> this may lead to seemingly contradictory results as observed for mimetic **6**. In the context of peptidomimetics, care must be taken not to over interpret CD spectroscopic data. A helical curve does not necessarily mean a rigid, highly constrained helical structure. NMR analysis of peptides that are conformationally dynamic yet spend a significant proportion of their time in a helical conformation can give rise to NOE cross peaks that suggest only a helical structure. It is therefore important to evaluate secondary structure using both methods. However, we found that NMR provides more useful structural information that can be used to rationalize biological data.

## 4 | CONCLUSIONS

The voltage gated sodium channels comprise a variety of related proteins with distinct physiological and pharmacological properties with specific subtypes localized to brain regions, skeletal muscle, peripheral neurons, and heart. Local anesthetic drugs work by blocking these channels and interrupting the flow of action potentials in neurons carrying nociceptive (and other sensory) information from the periphery to the central nervous system. The  $\mu$ -conotoxins present an opportunity to create safe, selective anesthetics but in their native form these peptides are unlikely to become lead drug compounds due to their unfavorable physicochemical properties.

In this work, we produced simplified structures based on  $\mu$ -KIIIA by removing the complex disulfide-bonding network and replacing it with chemical staple conformational constraints. We synthesized seven stapled mimetics using a variety of chemistries and compared them to the native  $\mu$ -KIIIA isomers as well as three nonstapled control compounds. Only compounds containing the  $i,i + 7$  staples (**3-5**) gave low micromolar inhibition of the two tested human sodium channels,  $\text{Na}_V1.4$ , from skeletal muscle and  $\text{Na}_V1.6$  from the CNS. Interestingly,

the reduced hydrocarbon-staple **5** could inhibit both  $\text{hNa}_V1.4$  and  $\text{hNa}_V1.6$  channels equally well, whereas the *trans*-staple **3** showed good inhibition of  $\text{Na}_V1.4$  but not  $\text{Na}_V1.6$ , indicating this compound could be used to selectively target one channel. The *cis*-staple **4** was also active, but significantly less than the other two mimetics, having a less favorable interaction with the binding sites. None of the other mimetics or controls were active, indicating that the structure of these compounds is key to biological activity. This was surprising, as Khoo *et al.*<sup>[29]</sup> had previously shown lactam-staple **9** to be active in rodent  $\text{Na}_V1.4$  and  $\text{Na}_V1.6$  channels. This species difference in receptor pharmacology highlights the importance of testing compounds using human VGSC assays in drug discovery programmes.

As the native  $\mu$ -KIIIA adopts an  $\alpha$ -helical conformation due to the complex disulfide-bonding network, we explored the secondary structure of our mimetics using CD. The data indicate little correlation between the CD peptide helicity and biological activity. Thus, we decided to examine the two most active mimetics **3** and **5** as well as the most helical  $i,i + 4$  staple (the *cis*-staple **6**), (according to CD), using solution NMR spectroscopy.

The two active mimetics **3** and **5** have similar structures to the native  $\mu$ -KIIIA helix, but at the C-termini the stapled peptides' backbones continue the helical trajectory where the native structure unwinds. As a result, the positioning of the backbone atoms of the linker residue that substitutes S13 and of R14 deviate significantly from those in the native structure, possibly explaining the lower activity of the mimetics. The NMR spectra of the *cis*-stapled mimetic **6** indicate that the compound was not stabilized in a well-defined conformation.

With an understanding of the structure-activity relationship of these peptidomimetics, our future investigations will focus on developing potent, selective human  $\text{Na}_V$ -channel blockers.

## ACKNOWLEDGMENTS

We thank the University of Glasgow, DSTL (Research Project Contract DSTL/AGR/R/CBRN/01) and EPSRC (EP/R511705/1) for financial support of this research. The authors also thank Andrew Monaghan (high-resolution mass spectrometry) and Dr Sharon Kelly (circular dichroism) for technical assistance.

## CONFLICT OF INTERESTS

There are no conflicts to declare.

## DATA AVAILABILITY STATEMENT

The Supporting Information is available free of charge on the Wiley publications website at <https://doi.org/10.1002/pep2.24203>. Experimental procedures and characterization data for all compounds, NMR spectra, Patch-clamp assay and analytical HPLC traces for final compounds.

## ORCID

Andrew G. Jamieson  <https://orcid.org/0000-0003-1726-7353>

## REFERENCES

- [1] W. J. Clench, Y. Kondo, *Am. J. Trop. Med. Hyg.* **1943**, *1*, 105.

- [2] D. Fegan, D. Andresen, *Lancet* **1997**, 349, 1672.
- [3] R. D. Rice, B. W. Halstead, *Toxicon* **1968**, 5, 223.
- [4] P. D. Anderson, G. Bokor, *J. Bioterror. Biodef.* **2012**, 3, 1.
- [5] K. B. Akondi, M. Muttenthaler, S. Dutertre, Q. Kaas, D. J. Craik, R. J. Lewis, P. F. Alewood, *Chem. Rev.* **2014**, 114, 5815.
- [6] A.-H. Jin, M. Muttenthaler, S. Dutertre, S. W. A. Himaya, Q. Kaas, D. J. Craik, R. J. Lewis, P. F. Alewood, *Chem. Rev.* **2019**, 119(21), 11510.
- [7] B. Gao, C. Peng, J. Yang, Y. Yi, J. Zhang, Q. Shi, *Toxins* **2017**, 9, 397.
- [8] G. C. Clark, N. R. Casewell, C. T. Elliott, A. L. Harvey, A. G. Jamieson, P. N. Strong, A. D. Turner, *Trends Biochem. Sci.* **2019**, 44, 365.
- [9] C. Netirojjanakul, L. P. Miranda, *Curr. Opin. Chem. Biol.* **2017**, 38, 70.
- [10] M. E. Brookes, S. Eldabe, A. Batterham, *Curr. Neuropharmacol.* **2017**, 15, 217.
- [11] P. J. Duggan, K. L. Tuck, *Toxins* **2015**, 7, 4175.
- [12] G. Bulaj, P. J. West, J. E. Garrett, M. Watkins, M.-M. Zhang, R. S. Norton, B. J. Smith, D. Yoshikami, B. M. Olivera, *Biochemistry* **2005**, 44, 7259.
- [13] H. Y. Frank, W. A. Catterall, *Genome Biol.* **2003**, 4, 207.
- [14] X. Pan, Z. Li, Q. Zhou, H. Shen, K. Wu, X. Huang, J. Chen, J. Zhang, X. Zhu, J. Lei, W. Xiong, H. Gong, B. Xiao, N. Yan, *Science* **2018**, 362 (6412), eaau2486.
- [15] X. Pan, Z. Li, X. Huang, G. Huang, S. Gao, H. Shen, L. Liu, J. Lei, N. Yan, *Science* **2019**, 363, 1309.
- [16] H. Shen, D. Liu, K. Wu, J. Lei, N. Yan, *Science* **2019**, 363, 1303.
- [17] S. D. Dib-Hajj, Y. Yang, J. A. Black, S. G. Waxman, *Nat. Rev. Neurosci.* **2013**, 14, 49.
- [18] A. Van Der Haegen, S. Peigneur, J. Tytgat, *FEBS J.* **2011**, 278, 3408.
- [19] M. Stevens, S. Peigneur, N. Dyubankova, E. Lescrinier, P. Herdewijn, J. Tytgat, *J. Biol. Chem.* **2012**, 287, 31382.
- [20] C. I. Schroeder, D. Adams, L. Thomas, P. F. Alewood, R. J. Lewis, *Biopolymers* **2012**, 98, 161.
- [21] S. Peigneur, O. Cheneval, M. Maiti, E. Leipold, S. H. Heinemann, E. Lescrinier, P. Herdewijn, M. E. De Lima, D. J. Craik, C. I. Schroeder, J. Tytgat, *FASEB J.* **2019**, 33, 3693.
- [22] R. M. Brady, M. Zhang, R. Gable, R. S. Norton, J. B. Baell, *Bioorg. Med. Chem. Lett.* **2013**, 23, 4892.
- [23] K. K. Khoo, M. J. Wilson, B. J. Smith, M.-M. Zhang, J. Gulyas, D. Yoshikami, J. E. Rivier, G. Bulaj, R. S. Norton, *J. Med. Chem.* **2011**, 54, 7558.
- [24] J. Tan, D. M. Soderlund, *Neurotoxicology* **2009**, 30, 81.
- [25] M. J. Thrippleton, J. Keeler, *Angew. Chem. Int. Ed. Engl.* **2003**, 42, 3938.
- [26] W. F. Vranken, W. Boucher, T. J. Stevens, R. H. Fogh, A. Pajon, M. Llinas, E. L. Ulrich, J. L. Markley, J. Ionides, E. D. Laue, *Proteins* **2005**, 59, 687.
- [27] J. P. Linge, M. Habeck, W. Rieping, M. Nilges, *Bioinformatics* **2003**, 19, 315.
- [28] J. P. Linge, M. A. Williams, C. A. Spronk, A. M. J. J. Bonvin, M. Nilges, *Proteins* **2003**, 50, 496.
- [29] K. K. Khoo, K. Gupta, B. R. Green, M.-M. Zhang, M. Watkins, B. M. Olivera, P. Balaram, D. Yoshikami, G. Bulaj, R. S. Norton, *Biochemistry* **2012**, 51, 9826.
- [30] A. G. Jamieson, N. S. Robertson, *Rep. Org. Chem.* **2018**, 5, 65.
- [31] M.-M. Zhang, B. R. Green, P. Catlin, B. Fiedler, L. Azam, A. Chadwick, H. Terlau, J. R. McArthur, R. J. French, J. Gulyas, *J. Bio. Chem.* **2007**, 282, 30699.
- [32] Y.-W. Kim, T. N. Grossmann, G. L. Verdine, *Nat. Protoc.* **2011**, 6, 761.
- [33] L. McDougall, A. G. Jamieson, *Stapled Peptides as Potential Therapeutics*, John Wiley & Sons, Ltd, Chichester **2019**.
- [34] C. E. Schafmeister, J. Po, G. L. Verdine, *J. Am. Chem. Soc.* **2000**, 122, 5891.
- [35] B. Aillard, N. S. Robertson, A. R. Baldwin, S. Robins, A. G. Jamieson, *Org. Biomol. Chem.* **2014**, 12, 8775.
- [36] N. J. Greenfield, *Nat. Protoc.* **2006**, 1, 2876.
- [37] S. Pacifico, A. Kerckhoffs, A. J. Fallow, R. E. Foreman, R. Guerrini, J. McDonald, D. G. Lambert, A. G. Jamieson, *Org. Biomol. Chem.* **2017**, 15, 4704.
- [38] A. Knuhtsen, C. Whitmore, F. S. McWhinnie, L. McDougall, R. Whiting, B. O. Smith, C. M. Timperley, A. C. Green, K. I. Kinnear, A. G. Jamieson, *Chem. Sci.* **2019**, 10, 1671.
- [39] R. S. Norton, *Modern Magnetic Resonance*, Springer, Cham **2017**, p. 1.
- [40] N. Purdie, H. G. Brittain, *Analytical applications of circular dichroism*, Elsevier, Oxford, UK **1993**.

#### SUPPORTING INFORMATION

Additional supporting information may be found online in the Supporting Information section at the end of this article.

**How to cite this article:** Knuhtsen A, Whiting R, McWhinnie FS, et al.  $\mu$ -Conotoxin KIIIA peptidomimetics that block human voltage-gated sodium channels. *Peptide Science*. 2021;113:e24203. <https://doi.org/10.1002/pep2.24203>